Extending the Vostok ice-core record of palaeoclimate to the penultimate glacial period

J. Jouzel*†, N. I. Barkov‡, J. M. Barnola§, M. Bender||†, J. Chappellaz§, C. Genthon§, V. M. Kotlyakov¶, V. Lipenkov‡, C. Lorius§, J. R. Petit§*, D. Raynaud§, G. Raisbeck#, C. Ritz§, T. Sowers||, M. Stievenard*, F. Yiou# & P. Yiou*

* Laboratoire de Modélisation du Climat et de l'Environnement, CEA/DSM CE Saclay, 91191, Gif sur Yvette Cedex, France
‡ Arctic and Antarctic Research Institute, Beringa Street 38, 199226, St Petersburg, Russia
§ Laboratoire de Glaciologie et Géophysique de l'Environnement, CNRS, BP96, 38402, Saint Martin d'Hères Cedex, France
|| Graduate School of Oceanography, University of Rhode Island, Narragansett, Rhode Island 02882-1197, USA
¶ Institute of Geography, Staromonetny, per 29, 109017, Moscow, Russia
# Centre de Spectrométrie Nucléaire et de Spectrométrie de Masse, 91405, Orsay, France

The ice-core record of local temperature, dust accumulation and air composition at Vostok station, Antarctica, now extends back to the penultimate glacial period (~140–200 kyr ago) and the end of the preceding interglacial. This yields a new glaciological timescale for the whole record, which is consistent with ocean records. Temperatures at Vostok appear to have been more uniformly cold in the penultimate glacial period than in the most recent one. Concentrations of CO_2 and CH_4 correlate well with temperature throughout the record.

In 1985 Lorius *et al.*[1] presented the first ice-core climate record spanning a full glacial–interglacial cycle. The record, which went back to the end of the penultimate glacial period about 150,000 years ago (150 kyr before present, BP) was based on ice drilled at Vostok, the Russian station in central East Antarctica (78° 28′ S and 106° 48′ E, mean annual temperature −55 °C, elevation 3,490 m). The Vostok records show that East Antarctica was colder and drier during glacial periods than during the Holocene[1–4], demonstrate that the large-scale atmospheric circulation was more vigorous during glacial times[5,6], support evidence from deep-sea sediment studies for orbital forcing of Pleistocene climate[2,7] and reveal direct correlations of carbon dioxide and methane concentrations with temperature. The last point suggests that variations in greenhouse gas concentrations have contributed to glacial–interglacial changes in climate[8–11]. Most of this work was based on the study of ice from the surface to 2,083 m depth in the 3Γ core.

Here we extend the record of Vostok geochemistry to the bottom of a new core, 4Γ, drilled down to 2,546 m. We include details of deuterium and dust concentrations measured in the ice and three parameters measured in the air bubbles entrapped in the ice: CO_2, CH_4 and the oxygen isotope ratio (given as $\delta^{18}O$) of O_2. Each parameter contains climate-related information. The new results (Table 1) are plotted against depth in Fig. 1, along with data from the bottom part of core 3Γ. The shallowest depth plotted, 1,500 m, corresponds to the end of the last interglacial period (LIG) and is dated at about 110 kyr BP. In addition, we will use information on changes in accumulation rate at Vostok contained in a new ^{10}Be profile also measured down to 2,546 m. Details on experimental procedures may be found elsewhere[2,6,8,9,12,13]. The depth profiles of CO_2, CH_4 and $\delta^{18}O$ in O_2 will undoubtedly evolve as additional samples are analysed.

We first describe a new timescale for the entire Vostok core. After discussing the reconstructed Vostok temperature record, we test our chronology by comparing various Vostok climate records with climate records from deep-sea sediments and, where relevant, curve of insolation. We then discuss the climate information contained in our new data set which covers the entire penultimate glacial period and extends through a part of the next to last interglacial down to ≃220 kyr BP.

Extending the glaciological dating approach

To interpret the Vostok data, we need a chronology for the ice, expressed as a curve of age against depth. We derive this chronology from the following four assumptions. First, the accumulation rate at Vostok has varied in the past as the derivative of the water vapour saturation pressure with respect to temperature at the level where the precipitation forms; that is, above the inversion layer[1,14]. Second, the accumulation (A) upstream of Vostok, where ice found at depth originates, increases with distance upstream according to $A(x)/A(x=0) = 1.00 + 0.65(x/X)$, where x is distance upstream of Vostok and X is distance of site Dome B upstream of Vostok (320 km). This equation invokes the observation that the Holocene as reflected by the δD or $\delta^{18}O$ records starts at a depth of ~300 m at Vostok and ~500 m at Dome B[15]. Third, ice at a depth of 1,534 m has an age of 110 kyr BP[16,17]. Finally, the strain-induced thinning of annual layers with depth is accurately described by the two-dimensional glaciological model of Ritz[18].

With these assumptions, we calculate the accumulation rate at Vostok today to be 1.98 g cm^{-2} yr^{-1}, 13% lower than the value of 2.3 g cm^{-2} yr^{-1} (ref. 1) based on estimates over the past 10 years, but in good agreement with the value of 2.00 ± 0.4 g cm^{-2} yr^{-1} estimated over the past 170 years using the Tambora eruption as a marker[19]. Back to 110 kyr BP, the biggest discrepancy with the chronology of Lorius *et al.*[1] is 3.5 kyr (Fig. 2). The age of the bottom of the core is 220 kyr BP. We refer to our age–depth curve as the 'extended glaciological timescale' (EGT). The uncertainty in the age of the bottom of the 4Γ core (2,546 m), largely dominated by the uncertainty in the current accumulation rate[18], is estimated to be ±20 kyr.

† J.J. is also at the Laboratoire de Glaciologie et Géophysique de l'Environnement. M.B. is on sabbatical leave at the Centre des Faibles Radioactivités, CNRS-CEA 91198, Gif-sur-Yvette Cedex, France.

Raisbeck *et al.*[13] obtained ^{10}Be concentrations in Vostok and have subsequently analysed the 3Γ and 4Γ cores in higher resolution (Raisbeck *et al.*, manuscript in preparation). We have used these data to calculate a curve of accumulation rate against depth for Vostok, assuming that the ^{10}Be deposition rate is constant and the same as the average value observed over the top 1,534 m (as above, we assume an age of 110 kyr BP for this depth). Complications that might introduce errors in such an estimate of accumulation are discussed in refs 20 and 21. Combining this accumulation rate with the flow model used above, we can calculate a ^{10}Be chronology which differs by no more than ~5 kyr from the EGT (Fig. 2). Although we believe this concordance tends to support the overall correctness of the EGT, it does not preclude significant differences in detail, particularly over periods when there were important climatic changes. For example, this ^{10}Be chronology gives a duration for the Holocene ~30% shorter than that given by the EGT.

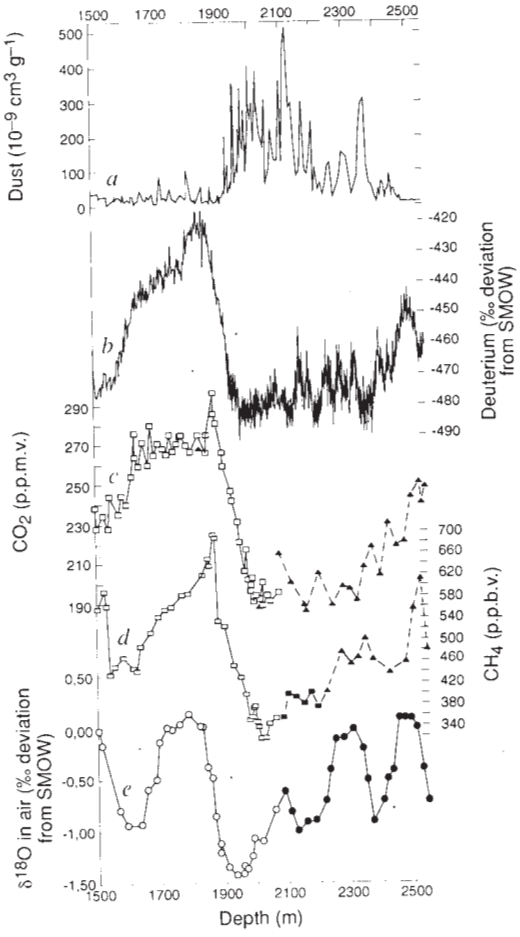

FIG. 1 Depth profiles *a*, Dust concentration. Data are from core 3Γ down to 2,200 m (6) and from core 4Γ below (discontinuous measurements every ~8 m). *b*, Deuterium content (δD in ‰ deviation from SMOW). In core 4Γ, δD was measured continuously below 1,920 m on 1-m ice increments down to 2,200 m (~150 yr), at higher resolution (0.5 m, ~70 yr) down to 2,414 m, and on 1-m increments from this depth down to 2,546 m. Data from 3Γ are reported for the 1,800–2,083-m depth interval. The agreement between 3Γ and 4Γ profiles is excellent over their common part. The comparison shows that there is no sizeable age difference between similar depth horizons in the cores despite small differences in the inclination of the two holes. *c*, *d*, *e*, Concentrations of CO_2, CH_4 and $\delta^{18}O$ of O_2 within air bubbles. Individual measurements are indicated by symbols: open symbols correspond to published data, and filled symbols to new data; for CH_4, squares and triangles correspond to different sets of measurements. Filled symbols are joined by a dotted line because the bottom part of the profile will undoubtedly evolve as additional samples are analysed.

The isotope temperature record

Precipitation is isotopically enriched with respect to atmospheric water vapour, and the vapour remaining in a given air mass is depleted at each condensation step both in δD and δ^{18}O. Simple models[22,23] predict that δ should vary linearly with temperature, T, in mid- and high latitudes. This predicted dependence is well documented from observations of present-day Antarctic precipitation[24,25]. We use the modern δ-T relationship to translate the δ change observed going back in time, at one given location, into a curve of temperature against age. This approach is supported by results from the general climate model studies[26,27] and independent glaciological estimates of glacial–interglacial temperature changes[28].

Temperature reconstructed from the isotopic profile is plotted against EGT age in Fig. 3 (curve 3*b*). We calculate the change from the present temperature using the equation $\Delta T_a = (1\ ^\circ C \text{ per } 9‰) \times (\delta D_{ice} - 8\delta^{18}O_{sw})$. T_a is the temperature immediately above the inversion layer where Antarctic precipitation forms[14]. The first term on the right is the inverse of the dependence of δD on temperature observed for this sector of East Antarctica[24], and the $8\delta^{18}O_{sw}$ term corrects for the variation of δD with ice volume[29]. The variation of $\delta^{18}O_{sw}$ as a function of Vostok age is taken from Sowers *et al.*[16].

The new record shows a long cold period from ~140 to 200 kyr BP. During this cold period, the amplitude of temperature variation is smaller than during the last ice age. In central Antarctica this entire period was nearly as cold as the Last Glacial Maximum (LGM) (~6 °C colder than the Holocene). Temperature is warmer before ~200 kyr BP, with a well marked peak around 215 kyr BP.

Correlating Vostok and oceanic records

We now extend to the bottom of the core the previous efforts to correlate the Vostok and the SPECMAP timescales by curve-matching records of temperature[17,30], dust[6], and δ^{18}O of O_2 and sea water[12,16]. We plot changes in the isotopic composition of sea water, and hence inferred continental ice volume, against age (curve 3*e*).

The Vostok temperature record compares well with sea surface temperature (SST) in various Indian ocean cores[17,30]. For example, in the summer SST record of RC11-120 (ref. 31), stages 7.1 and 7.3 are colder than the Holocene and much colder than

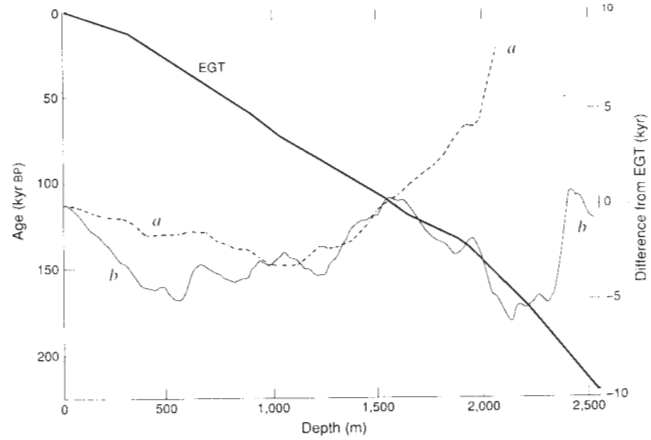

FIG. 2 The depth–age relationship for the EGT, together with differences between this and (*a*) the original timescale of Lorius *et al.*[1], and (*b*) the '^{10}Be' timescale derived assuming a constant ^{10}Be flux and assigning the 110-kyr BP level at 1,534 m. Differences (right scale) are negative when the EGT gives older ages.

TABLE 1 Carbon dioxide, methane and oxygen

CO_2 (p.p.m.v.)			CH_4 (p.p.b.v.)			$\delta^{18}O$ (‰)		
Depth (m)	Age (kyr)	Mean	Depth (m)	Age (kyr)	Mean	Depth (m)	Age (kyr)	Mean
2078	150.1	197.7	2089	151.5	356	2089	151.6	0.60
2116	155.4	192.6	2102	153.6	400	2101	153.4	0.74
2157	160.3	189.7	2127	156.7	395	2109	154.5	0.82
2164	161.4	186.2	2153	159.8	382	2129	157.0	0.98
2203	166.9	205.1	2177	163.5	403	2139	158.1	0.89
2225	169.6	192.3	2196	166.1	376	2158	160.5	0.88
2247	172.9	184.5	2225	169.6	405	2167	161.9	0.80
2280	177.8	198.6	2273	176.9	478	2188	165.0	0.87
2302	180.9	198.5	2302	180.9	456	2198	166.3	0.79
2325	184.1	191.0	2325	184.1	468	2220	169.0	0.66
2333	185.3	190.8	2348	187.5	503	2233	170.7	0.38
2348	187.5	208.5	2373	191.1	464	2251	173.6	0.09
2363	189.6	214.0	2425	199.8	440	2278	177.6	0.11
2372	190.9	218.5	2475	207.5	460	2290	179.2	−0.13
2386	193.1	200.5	2501	211.5	558	2298	180.4	−0.10
2399	195.2	204.2	2525	214.9	612	2309	181.9	0.04
2414	197.9	211.5	2543	217.5	482	2329	184.7	−0.01
2425	199.8	232.2				2338	186.1	0.24
2437	201.6	232.3				2350	187.9	0.47
2451	203.7	218.8				2369	190.5	0.88
2475	207.5	220.9				2388	193.4	0.87
2499	211.2	243.5				2402	195.7	0.72
2525	214.9	251.9				2413	197.6	0.53
2533	216.0	240.0				2423	199.4	0.47
2543	217.5	248.6				2433	201.0	0.38
						2441	202.2	0.12
						2452	203.9	−0.11
						2462	205.5	−0.03
						2469	206.6	−0.11
						2489	209.7	−0.14
						2500	211.3	−0.06
						2510	212.7	0.04
						2518	213.8	0.20
						2528	215.3	0.39
						2544	217.6	0.66

The deuterium and dust data are available from the authors on request.

the Last Interglacial (curve 3*a*), in agreement with the Vostok temperature record. Correlating the Vostok temperature peak at 215 kyr BP with the RC11-120 peak at 218 kyr BP suggests that the bottom of the Vostok core corresponds to marine stage 7.4. The comparison with RC11-120 thus supports our glaciological timescale.

The dust concentration is plotted against EGT age in curve 3*g*. High values are observed throughout the penultimate glacial period (140–200 kyr BP). There is a small maximum at about 160 kyr BP and a broad minimum between 170 and 190 kyr BP. Low values are recorded before 200 kyr BP, consistent with our interpretation that this depth interval lies in the stage 7 interglacial period. We compare dust concentration at Vostok and the mass accumulation rate (MAR) in core RC27-61 from the Indian Ocean which gives a good record of aeolian input[32]. Both (curve 3*f*) are highest during glacial stages (2, 4 and 6), and low during the interglacial stages (1, 5 and 7). The two records are almost always in phase to within ±10 kyr; the exception is between 170–190 kyr, where the low values in Vostok have no parallel in the RC27-61 record. At around 200 kyr BP, dust rises at Vostok 10 kyr before MAR rises at RC27-61, and at 145 kyr BP decreases at Vostok again about 10 kyr before the MAR decreases at RC 27-61. It is not clear whether these differences reflect errors in the chronologies or true differences in phasing.

The $\delta^{18}O$ of past atmospheric O_2 is plotted against EGT age in curve 3*d*, after correction for differences between gas age and ice age[33], and for gravitational fractionation[34]. Variations of $\delta^{18}O$ of O_2 are governed mainly by processes associated with oxygen isotope exchange of O_2 and sea water due to photosynthesis and respiration[35]. These variations are thought to be closely related to variations in the $\delta^{18}O$ of sea water: when the composition of sea water changes, the composition of O_2 produced by photosynthesis changes, transmitting the sea water variations to the atmospheric O_2 reservoir[36]. For the sake of simplicity, we do not consider the small additional variations in the $\delta^{18}O$ of O_2 associated with glacial–interglacial variations in oxygen isotope fractionation by biogeochemical and hydrologic processes[16] (that is, changes in the Dole effect).

The record of variations in $\delta^{18}O$ of O_2 looks similar to the record of variations in $\delta^{18}O$ of sea water (curve 3*e*). It also resembles the curve of June insolation at 20° N (curve 3*c*), because variations in $\delta^{18}O$ of sea water and variations in the Dole effect are both linked to insolation. We therefore test the EGT chronology by comparing $\delta^{18}O$ of O_2 with $\delta^{18}O$ of sea water and with insolation. Uncertainties restrict the comparison to about ±10 kyr; within this uncertainty, variations in $\delta^{18}O$ of O_2 as dated by the EGT chronology are consistent with sea water $\delta^{18}O$ and insolation curve. Thus the $\delta^{18}O$ measurements, as well

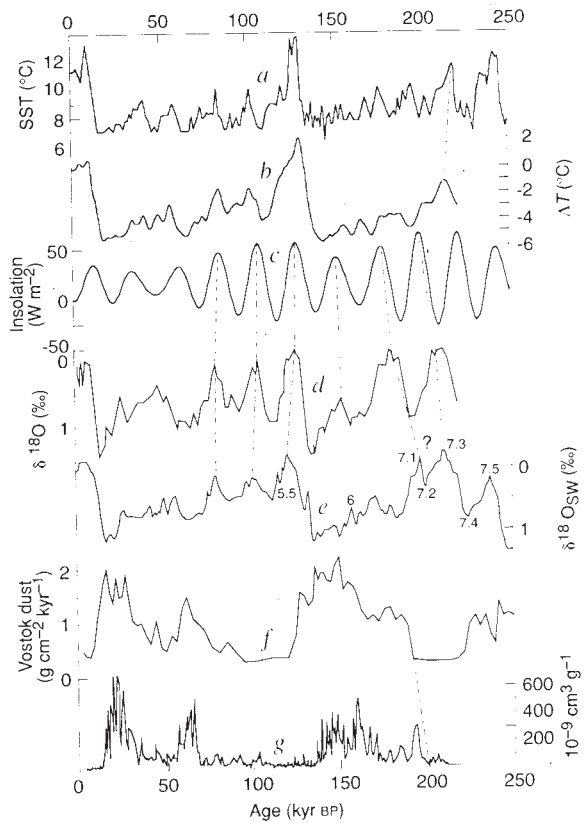

FIG. 3 Variations with time. *a*, Summer sea surface temperature (SST) at Indian Ocean site RC11-120 (16° 37′ N, 59° 52′ E). *b*, Atmospheric temperature change at Vostok (above the inversion) as derived from the deuterium profile. We used published deuterium data down to 1,920 m (ref. 2) and extended this record down to 2,083 m by averaging 3Γ and 4Γ data and to 2,546 m using 4Γ data alone; we then smoothed the entire record. *c*, Summer insolation at 20° N (ref. 49). *d*, $\delta^{18}O$ of O_2 measured in the air bubbles on the EGT. *e*, Change in the isotopic composition of sea water derived from the V19-30 $\delta^{18}O$ foraminifera record and extended back to 250 kyr BP[16]; the record is normalized so that the average Holocene value is 0‰. *f*, Mass accumulation rate (MAR) in the Indian Ocean site RC27-61 (adapted from ref. 32). *g*, The dust concentration in the Vostok ice. The Vostok records are reported using the EGT and the deep-sea records using the SPECMAP[31] timescale. Horizons in the Vostok and deep-sea cores which are believed to be correlative are joined by dotted lines (see text).

as dust and temperature comparisons, support the EGT chronology.

The duration of the Last Interglacial, now highly controversial, is crucial for new insights on the causes of glacial–interglacial cycles[37–39]. Relevant information is summarized in Fig. 4. Here we plot the Vostok temperature record using the adopted EGT and other timescales which would be derived from different starting assumptions. In the figure, we also show the $\delta^{18}O$ of sea water, the curve of sea surface temperature derived from core MD 84-551 (ref. 17) and the recently published[37] isotopic record of vein calcite from Devils Hole (Nevada). The LIG lasts twice as long at Vostok in the chronology of Lorius *et al.* than in the deep-sea record of the sea-level change[1,2].

Both the use of air $\delta^{18}O$ (ref. 16) and the correlation with Southern Ocean SST[17] have recently confirmed that the temperature at Vostok rose before (~5 kyr at mid-transition) sea level rose for this termination (termination 2). As the EGT is, at mid-transition, ~4 kyr younger than that of Lorius *et al.*, the EGT and SPECMAP timescales now appear in agreement for this termination 2 (but differences of up to 6 kyr still exist at the LIG peak). The EGT timescale supports the observation, now well documented, that the duration of this interglacial is longer in the Vostok temperature and Southern Ocean SST records than in the record of sea-level change. This conclusion is fairly insensitive to our assumption about Vostok age at 1,534 m depth (a 5% change in age at 110 kyr BP will modify the duration by only 1 kyr or so). The duration which would be derived from the ^{10}Be chronology is similar, within 2 kyr, to that obtained with the EGT (but note the uncertainties of the ^{10}Be method mentioned above). Finally, the Vostok and Devils Hole records[37] agree less convincingly with the EGT than with the timescale of Lorius *et al.*[1].

Climate Interpretation

We now examine how the extension of the records, and the new information they contain, complement or modify our current climatic interpretation of Vostok data. In turn, we discuss the dust record, the link between orbital forcing and climate, and the record of greenhouse-gas concentrations.

The dust throughout the Vostok record begins to increase rapidly when Vostok atmospheric temperature drops by more than ~4 °C below its modern value. We interpret this result as indicating that the penultimate glacial period, like the last glacial period, was characterized by more extensive deserts, more intense surface winds in the desert source regions and/or more efficient meridional transport. The isotopic composition from the LGM dust in the Dome C core[40] suggests that the Patagonia desert might be the main contributor to dust fallout in East Antarctica. During the end of the previous interglacial, as during the LIG and today, dust fallout was very low.

An intriguing feature of the records is that dust at Vostok covaries so closely with Vostok isotopic temperature whereas MAR at RC27-61 covaries so closely with sea water $\delta^{18}O$. The dust record is similar to the record of mass accumulation rate for the Northern Hemisphere Indian Ocean core RC27-61. Over the entire Vostok record, there are similarities between dust and indicators of dust source strength in Central Asia analysed in Chinese loesses[41,42]. These similarities indicate that large-scale changes in dust fallout reflect global changes in climate.

We examine the link between Vostok temperature and orbital forcing through spectral analysis using a multi-taper method[7,43]. The analysis was done (1) for the entire 2,546-m record, and (2) for the same series limited to 2,083 m using either the EGT or the Lorius *et al.* timescale. Using the EGT instead of the chronology of Lorius *et al.* causes a slight shift in the period of the obliquity peak (from 41.7 to 40.3 kyr), retains the strong significance of this peak and makes the significance of the precessional peak stronger, probably because of the shortening of the LIG. Using the full time series (EGT chronology) leads to a decrease in the amplitude of the obliquity peak (41.01 kyr) which is even more significant; but the precessional peak (24.6 kyr) is now weaker and less significant. This decrease in amplitude of orbital frequencies is the quantitative expression of uniformly cold temperatures throughout the period between 140–200 kyr BP. During most of the record there is a strong relationship between local annual insolation, which primarily reflects obliquity, and temperature[2]. This relationship is absent, however, between 140 and 200 kyr BP: the insolation maximum at ~170 kyr BP has no clear temperature counterpart.

Polar ice cores provide the most direct evidence of past changes in greenhouse gas concentrations. These changes are well documented for CO_2 and CH_4 and to a lesser degree for N_2O (ref. 44 for a review). Previously published results obtained on Vostok and other ice cores highlight the correlation between CO_2 concentration, CH_4 concentration and temperature throughout the last climate cycle. Results from Vostok also reveal phase differences between CO_2 and temperature. At the end of the penultimate interglacial, for example, the CO_2 decrease lags behind the Antarctic cooling leading to glacial conditions.

The CO_2 and CH_4 concentrations for the entire Vostok core profiles are plotted against age in Fig. 5 using the EGT after correction for the difference between gas age and ice age[33,45]. CO_2 concentrations are low during the penultimate glacial period, from 140 to 190 kyr BP. These values are similar to the

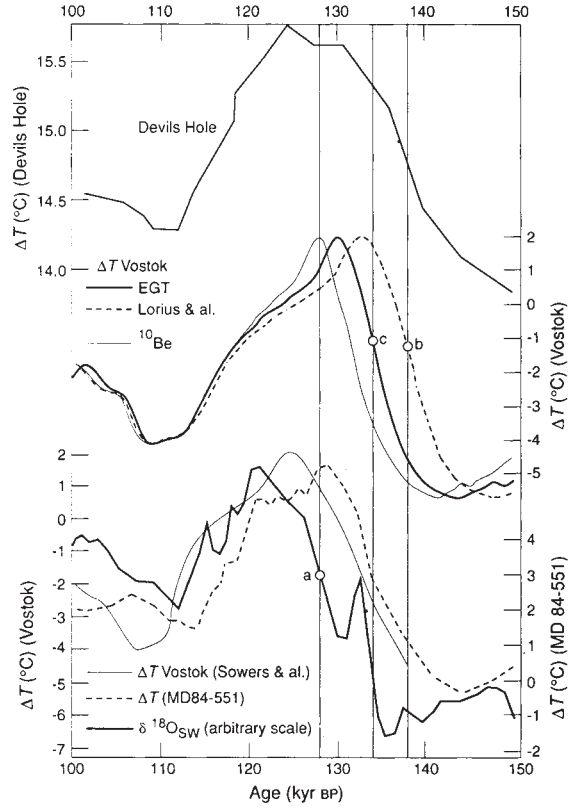

FIG. 4 The Vostok temperature record on various timescales for the 100–150 kyr BP period encompassing the LIG. Upper curve: the Devil's Hole record; middle curves: Vostok temperature using three different timescales ('^{10}Be', EGT and Lorius *et al.*); lower curves: Vostok temperature (using the timescale obtained by Sowers *et al.*[16] in correlating sea water $\delta^{18}O$ with ^{18}O of O_2); the sea surface temperature estimated from core MD84-551[17]; and the sea water $\delta^{18}O$ (similar to 3e with an arbitrary scale chosen in such a way this curve is comparable to the temperature records). The three vertical lines correspond to: a, mid-transition in sea water $\delta^{18}O$, a proxy of sea-level and ice volume change (128 kyr BP); b, mid-transition in Vostok temperature using the Lorius *et al.* timescale (138 kyr BP); and c, mid-transition according to the EGT reference timescale (134 kyr BP).

concentrations observed during the last glacial period between ~60 and 18 kyr BP. Before 190 kyr BP, the CO_2 values are higher. At the very bottom of the core, the CO_2 concentration is about 250 p.p.m.v., intermediate between full glacial concentrations and preindustrial values. The lowest CH_4 concentrations are similar to, or slightly lower than, those in the LGM, and are observed only during the final stage of the penultimate glaciation. The measurements are too scarce to discuss in detail this new part of the CH_4 record. Nevertheless, the increasing trend towards the bottom should be noted, especially the marked peak at the bottom with a maximum concentration of 610 p.p.b.v. Again, the concentrations measured near the very bottom are intermediate between full glacial and preindustrial values. This is consistent with the dating, indicating that the bottom ice is from the end of the previous interglacial period.

The strong covariation between CO_2 and temperature and CH_4 and temperature observed for the last 160 kyr is also present in the new part of the Vostok record. The CO_2–temperature correlation coefficient (r^2) over the past 220 kyr is 0.81 (0.76 for CH_4) instead of 0.78, in each case, over the last 160 kyr. In contrast to the lag of CO_2 behind temperature observed around 110 and 70 kyr BP, the CO_2 decrease between 220 and 190 kyr BP is in phase with the temperature change. A notable feature of the CH_4 results is the absence of clear oscillations during the penultimate glacial period. These would be expected from the link between the methane record and a monsoonal precipitation index largely dominated by the precession cycle[46] which was suggested for the past 160 kyr (ref. 9). This feature is directly reflected in the CH_4 spectrum: the amplitude and significance of the precession peak are smaller for the full record than for the last 160 kyr. The CO_2 spectrum also differs between the longer and shorter records, although in a different way. The 220-kyr CO_2 record now shows significant peaks at obliquity and both precession periodicities, whereas only the precession peak was present for the last climate cycle[7]. This also reflects, in the spectral domain, what is clearly seen in the CO_2 record: the long penultimate glacial period and the last ice age have different characteristics. Obviously, all these features would need to be confirmed by further measurements.

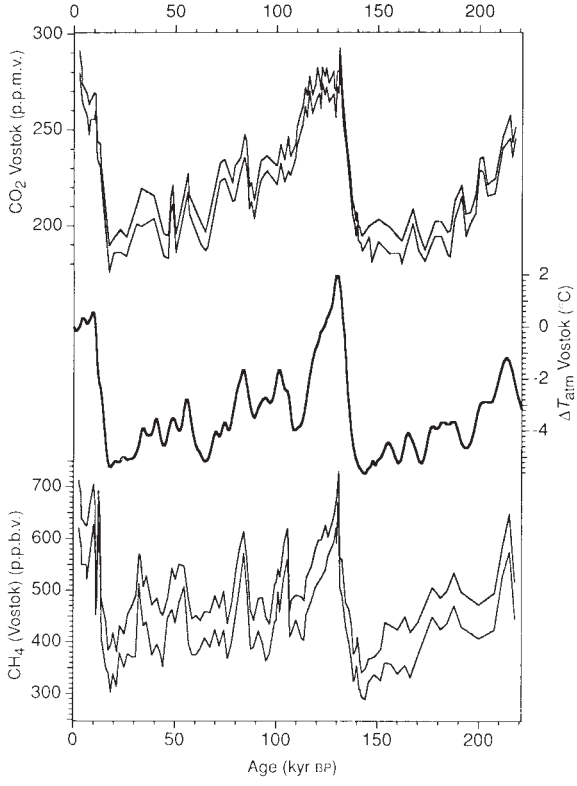

FIG. 5 CO_2, CH_4 and Vostok atmospheric temperature with respect to time (EGT) with the air–ice age difference calculated following Barnola *et al.*[33], taking into account the temperature dependence of the ice density[50]. For CO_2 and CH_4, the envelope corresponds to the measurement accuracy.

Conclusions

Our new chronology appears to correlate well with oceanic records. In particular, the EGT chronology resolves half of the 10-kyr discrepancy in the duration of the LIG that arose when the previous Vostok chronology was compared to the deep-sea record. With the EGT chronology, the duration of the LIG at Vostok is still 5 kyr longer than its duration in deep-sea sediments. We believe that this important difference reflects the fact that, during termination 2, Antarctic temperatures rose ~5 kyr before the Northern Hemisphere ice sheets began to melt[12,17]. In general, matching Vostok climate records with deep-sea sediments records and insolation curves supports our entire chronology to ±10 kyr.

The isotopic temperature record shows that there is a long cold period in East Antarctica which we date from about 140 to 200 kyr BP. The coldest isotopic temperatures measured during this period are similar to those measured during the last glacial maximum, but the duration of the cold period is much longer. Isotopic temperatures rise in the bottom of the Vostok 4Γ core corresponding to interstadial-interglacial periods of marine stage 7. The overall covariation of climate variables in the newly examined section of the Vostok ice core is similar to that observed for the last glacial–interglacial cycle[8,9]. Thus concentrations of CO_2 and CH_4 are lowest during the penultimate glacial period, where their values are comparable to those of the LGM. CO_2 and CH_4 are positively correlated with isotopic temperatures with correlations similar to those found during the last climate cycle. Throughout the record, dust concentrations at Vostok rise during cold periods, and are very low when temperatures are less than ~4 °C colder than modern values.

There is still much more climate information to extract from Vostok drilling. There is more than 1 km of ice below the 2,546 m reached by core 4Γ (the ice thickness is ~3,700 m), which may represent more than 500 kyr of time. At the same time, the new data discussed here, together with the results of the GRIP[47] and GISP2[48] cores, will allow comparison of climate change in Antarctica and Greenland beyond 200 kyr BP. □

Received 22 March; accepted 10 June 1993.

1. Lorius, C. *et al. Nature* **316,** 591–596 (1985).
2. Jouzel, J. *et al. Nature* **329,** 403–408 (1987).
3. Yiou, F., Raisbeck, G. M., Lorius, C. & Barkov, N. I. *Nature* **316,** 616–617 (1985).
4. Jouzel, J. *et al. Quat. Res.* **31,** 135–150 (1989).
5. De Angelis, M., Barkov, N. I. & Petrov, V. N. *Nature* **325,** 318–321 (1985).
6. Petit, J. R. *et al. Nature* **343,** 56–58 (1990).
7. Yiou, P. *et al. J. geophys. Res.* **96,** 20365–20378 (1991).
8. Barnola, J. M., Raynaud, D., Korotkevich, Y. S. & Lorius, C. *Nature* **329,** 408–414 (1987).
9. Chappellaz, J., Barnola, J. M., Raynaud, D., Korotkevich, Y. S. & Lorius, C. *Nature* **345,** 127–131 (1990).
10. Genthon, C. *et al. Nature* **329,** 414–418 (1987).
11. Lorius, C., Jouzel, J., Raynaud, D., Hansen, J. E. & Le Treut, H. *Nature* **347,** 139–145 (1990).
12. Sowers, T., Bender, M., Raynaud, D., Korotkevich, Y. S. & Orchado, J. *Paleoceanography* **6,** 679–696 (1991).
13. Raisbeck, G. M. *et al. Nature* **326,** 273–277 (1987).
14. Robin, G. de Q. *Phil. Trans. R. Soc.* B**280,** 143–148 (1977).
15. Vaikmae, R., Jouzel, J. & Petit, J. R., presentation at mtg on *Application of Isotope Techniques in Studying Past and Current Environmental Changes in the Hydrosphere and the Atmosphere*, Vienna, April 1993.
16. Sowers, T. *et al. Paleoceanography* (submitted).
17. Pichon, J. J. *et al. Paleoceanography* **7,** 289–318 (1992).
18. Ritz, C. *J. Glaciol.* (in the press).
19. Legrand, M. & Delmas, R. *Nature* **327,** 671–676 (1987).
20. Raisbeck, G. M. *et al. The Last Deglaciation: Absolute and Radiocarbon Chronologies* (eds Bard, E. & Broecker W.S.) 127–139 (NATO ASI Series I2, Springer, Berlin, 1992).
21. Raisbeck, G. M. & Yiou, F. *Nuclear Instrum. Meth.* B**5,** 91–99 (1984).
22. Dansgaard, W. *Tellus* **16,** 436–468 (1964).
23. Jouzel, J. & Merlivat, L. *J. geophys. Res.* **89,** 11749–11758 (1984).
24. Lorius, C. & Merlivat, L. *IAHS Publ.* **118,** 127–137 (1979).
25. Dahe, Q., Petit, J. R., Jouzel, J. & Stievenard, M. *J. Glaciol.* (in the press).
26. Joussaume, S. & Jouzel, J. *J. geophys. Res.* **98,** 2807–2830 (1993).

27. Jouzel, J., Koster, R. D., Suozzo, R. & Russell, G. *EOS* (Spring Meeting supplement, 7 April) (1992).
28. Johnsen, S. J. *et al. Nature* **359,** 311–313 (1992).
29. Craig, H. *Science* **133,** 1702–1703 (1961).
30. Shackleton, N. J., Mix, A. & Hall, M. A. *Quat. Sci. Rev.* **11,** 387–400 (1992).
31. Martinson, D. G. *et al. Quat. Res.* **27,** 1–29 (1987).
32. Clemens, S. & Prell, W. *Paleoceanography* **5,** 109–145 (1992).
33. Barnola, J. M., Pimentia, P., Raynaud, D. & Korotkevich, Y. S. *Tellus* B**43,** 83–90 (1991).
34. Craig, H., Horibe, Y. & Sowers, T. A. *Science* **242,** 1675–1678 (1988).
35. Dole, M., Lane, G. A., Rudd, D. P. & Zaukelies, D. A. *Geochim. cosmochim. Acta* **6,** 65–78 (1954).
36. Bender, M., Labeyrie, L. D., Raynaud, D. & Lorius, C. *Nature* **318,** 349–352 (1985).
37. Winograd, I. J. *et al. Science* **258,** 255–260 (1992).
38. Lambeck, K. & Nakada, M. *Nature* **357,** 125–128 (1992).
39. Imbrie, J., Mix, A. C. & Martinson, D. G. *Nature* **363,** 531–533 (1993).
40. Grousset, F. *et al. Earth planet. Sci. Lett.* **111,** 175–182 (1992).
41. Kukla, G., An, Z. S., Melice, J. L., Gavin, J. & Xiao, J. L. *Trans. R. Soc. Edin.* **81,** 263–288 (1990).
42. Beer, J. *et al. Geophys. Res. Lett.* **20,** 57–60 (1993).
43. Thomson, D. J. *Proc. IEEE* **70,** 1055–1096 (1982).
44. Raynaud, D. *et al. Science* **259,** 926–934 (1993).
45. Sowers, T. A., Bender, M. L., Raynaud, D. & Korotkevich, Y. L. *J. geophys. Res.* **97,** 15683–15697 (1992).
46. Prell, W. & Kutzbach, J. E. *J. geophys. Res.* **92,** 8411–8425 (1987).
47. Dansgaard, W. *et al. Nature* **364,** 218–220 (1993).
48. Taylor, K. T. *et al. Nature* **361,** 432–436 (1993).
49. Berger, A. L. *J. atmos. Sci.* **35,** 2362–2367 (1978).
50. Martinerie, P., Raynaud, D., Etheridge, D., Barnola, J. M. & Mazaudier, D. *Earth planet Sci. Lett.* **112,** 1–13 (1992).

ACKNOWLEDGEMENTS. Vostok is a joint project between Russia, France and the United States. We thank participants in drilling, field work and ice sampling. We acknowledge the Russian Antarctic Expeditions, the Institut Français de Recherches et Technologies Polaires and the NSF Division of Polar Programs for logistic support. The project is supported in Russia by the Russian Ministry of Sciences, in France by the Programme National d'Études de la Dynamique du Climat, Fondation de France and the Commission of European Communities Environment Programme, and in the U.S., by the NSF. We thank J. Meyssonnier for discussions, J. C. Pugno for the figures and C. Alba, P. Doira and M. Delmotte for isotope analyses.

Co-crystal structure of the HNF-3/*fork head* DNA-recognition motif resembles histone H5

Kirk L. Clark*†, Elaine D. Halay*†, Eseng Lai‡ & Stephen K. Burley*†§

* Laboratories of Molecular Biophysics and † Howard Hughes Medical Institute, The Rockefeller University, 1230 York Avenue, New York, New York 10021, USA
‡ Cell Biology and Genetics Program, and Endocrinology Service Memorial Sloan-Kettering Cancer Center, New York, New York 10021, USA

The three-dimensional structure of an HNF-3/*fork head* DNA-recognition motif complexed with DNA has been determined by X-ray crystallography at 2.5 Å resolution. This α/β protein binds B-DNA as a monomer, through interactions with the DNA backbone and through both direct and water-mediated major and minor groove base contacts, inducing a 13° bend. The transcription factor fold is very similar to the structure of histone H5. In its amino-terminal half, three α-helices adopt a compact structure that presents the third helix to the major groove. The remainder of the protein includes a twisted, antiparallel β-structure and random coil that interacts with the minor groove.

MEMBERS of the HNF-3/*fork head* family of eukaryotic transcription factors share a highly conserved DNA-binding domain and occur in various organisms ranging from yeast to man (reviewed in ref. 1). Hepatocyte nuclear factor-3 (HNF-3) proteins were first identified as activators of liver-specific gene expression in rat[2]. Initial evidence for a new DNA-binding motif came when HNF-3α, β and γ were found to share a novel, highly conserved DNA-binding region[3,4] with the nuclear protein product of the *Drosophila* homeotic *fork head* gene, involved in the formation of terminal structures of the early fly embryo[5,6].

Functionally significant HNF-3 binding sites were identified in the promoters of a large number of genes expressed in mammalian hepatocytes (for example, albumin[7], phosphoenolpyruvate carboxykinase[8] and two liver-specific transcription factors, HNF-1α (ref. 9) and HNF-3β (ref. 10)), indicating roles for HNF-3 in both cell differentiation and tissue-specific gene expression. Other members of the HNF-3/*fork head* family have also been implicated in development; *fork head* mutant embryos lack structures contributing cells to the fore- and hindgut of the fly[5]. The sloppy paired proteins (slp1 and slp2) affect fly segmentation[11]. XFKH1 is expressed in the blastopore-lip of *Xenopus* embryos and is essential for normal axis formation[12].

We now report the X-ray crystallographic structure determination of a canonical HNF-3/*fork head* DNA-recognition motif bound to its target DNA sequence. The three-dimensional structure of the DNA-binding domain of HNF-3γ bound to its cognate DNA, obtained at 2.5 Å resolution, reveals a monomeric α/β protein structure interacting with B-DNA. The N-terminal half of the polypeptide chain adopts a compact three-helix structure, which presents its third α-helix to the major groove. The carboxy-terminal half of the protein consists of β-strands and random coil and makes various DNA contacts. Elucidation of this DNA-recognition fold provides a three-dimensional scaffold with which to understand the DNA-binding properties of members of the HNF-3/*fork head* family of transcription factors. Structural comparisons demonstrate a striking similarity to an unrelated, DNA-packaging protein histone H5 (ref. 13).

Structure determination and refinement

A fragment of HNF-3γ, HNF-3γ(107–223), containing the conserved DNA-binding region, was expressed, purified and co-crystallized with a 13-base-pair (bp) duplex oligonucleotide bearing a sequence derived from its transthyretin (TTR) promoter binding site[2] (Fig. 1 and Table 1). Quantitative electrophoretic mobility shift (EMS) assays[2] documented specific nanomolar-affinity DNA binding of the purified recombinant protein with the sequence used for co-crystallization at a protein:

§ To whom correspondence should be addressed.